Editors' Suggestion

Single- and double-electron capture in intermediate-energy $N^{5+} + H_2$ collisions

Y. W. Zhang,[1] J. W. Gao,[2,*] Y. Wu,[1,3,†] F. Y. Zhou,[3] J. G. Wang,[3] N. Sisourat,[4] and A. Dubois[4]

[1]*Center for Applied Physics and Technology, HEDPS, and School of Physics, Peking University, 100871 Beijing, China*

[2]*Laser Fusion Research Center, China Academy of Engineering Physics, 621900 Mianyang, China*

[3]*Key Laboratory of Computational Physics, Institute of Applied Physics and Computational Mathematics, 100088 Beijing, China*

[4]*Sorbonne Université, CNRS, UMR 7614, Laboratoire de Chimie Physique-Matière et Rayonnement, 75005 Paris, France*

(Received 15 June 2020; accepted 28 July 2020; published 24 August 2020)

Single- and double-electron capture processes in $N^{5+} + H_2$ collisions are investigated in a broad energy domain ranging from 0.25 to 150 keV/u. Total and partial cross sections are calculated using a three-center, two-active-electron, semiclassical nonperturbative approach. For single-electron capture cross sections the present results show an excellent agreement below 10 keV/u where theoretical and experimental data are available and discriminate between them when disagreement exists. Furthermore, it is shown that the cross sections for double-electron capture into autoionizing states are particularly significant and thus contribute substantially to the total single-electron capture cross sections through postcollisional autoionization. The cross sections for double-electron capture processes into bound states of N^{3+} are also reported and show severe discrepancies with the rare available data.

DOI: 10.1103/PhysRevA.102.022814

I. INTRODUCTION

Over the past decades, electron capture processes induced by highly charged ions colliding with H_2 molecules have been studied extensively because of their great importance in various domains, such as the understanding of x-ray emission from solar wind ions interacting with cometary neutral species [1] and the modeling of fusion plasmas for diagnostic purposes [2]. For the system N^{5+}-H_2, a substantial number of experimental investigations [3–7] have been carried out for single-electron capture (SEC) processes [8],

$$N^{5+}(1s^2) + H_2(X\,^1\Sigma_g^+) \rightarrow N^{4+}(1s^2n\ell) + H_2^+(X\,^2\Sigma_g^+) \quad (1a)$$

$$\rightarrow N^{4+}(1s^2n\ell) + 2H^+ + e^- \quad (1b)$$

$$\rightarrow N^{4+}(1s^2n\ell) + H^+ + H(n'\ell'), \quad (1c)$$

where the latter two lead to H_2 dissociation and correspond to the bielectronic processes transfer-ionization and transfer-excitation. In contrast, only very few data are available for the double-electron capture (DEC) process [3],

$$N^{5+}(1s^2) + H_2(X\,^1\Sigma_g^+) \rightarrow N^{3+}(1s^22\ell n'\ell') + 2H^+. \quad (2)$$

In the latter equation, the $N^{3+}(1s^22\ell n'\ell')$ states lie under the first ionization threshold, $N^{4+}(1s^22s\ ^2S)$, and are thus bound. Conversely, DEC to autoionizing states (labeled ADC or AIDC in previous works and in the following) [9] reads

$$N^{5+}(1s^2) + H_2(X\,^1\Sigma_g^+) \rightarrow N^{3+}(1s^2n\ell n'\ell') + 2H^+, \quad (3)$$

with $n\ell = 2p$, $n' > 5$, and $n, n' > 3$ (see Table I). It should be noted here that the one- and two-electron processes listed in Eqs. (1) and Eq. (3) contribute to the same, so-called single-projectile charge-changing cross sections. The latter are termed total SEC in the following, while direct SEC is used for the three processes in Eqs. (1).

The previous experimental works have focused on collision energies below 10 keV/u where SEC to $N^{4+}(1s^23\ell, 1s^24\ell)$ and ADC to $N^{3+}(1s^23\ell n\ell')$ were shown to be the dominant processes. However, in the experiment [7], the ADC cross sections could not be extracted from those of SEC to $N^{4+}(1s^22\ell)$ due to the extremely short lifetime of double-excited autoionizing N^{3+} states [10,11].

From the theoretical point of view investigating this collision system remains challenging due to the strong coupling between various channels, the multicenter features of the H_2 molecular target, and the role of the electronic correlation, notably in the important two-electron processes invoked just above. Most of the previous theoretical investigations [12–15] have been based on single-active-electron and single-center target approaches concentrating on impact energies below 10 keV/u. There are discrepancies between these works and the experimental data, probably because of the neglect of the coupling with the most important two-electron processes, the lack of electronic correlation, and the use of the atomic model potential to describe the active electron interacting with the H_2^+ core. Errea *et al.* [16] revisited the study of $N^{5+} + H_2$ collisions for energies ranging from 0.01 to 10 keV/u using a two-active-electron, three-center, semiclassical, molecular-orbital close-coupling (SCMOCC) method. Reasonable agreement with some of the experimental SEC shell-selective cross sections was obtained. However, the channels correlating with SEC to $N^{4+}(4\ell, \ell > 0) + H_2^+(X\,^2\Sigma_g^+)$ were not considered in their calculations.

To date, one can state that despite extensive experimental and theoretical investigations of $N^{5+} + H_2$ collisions, there are still large discrepancies between the available results. Furthermore, there is only a single experimental investigation

*gwen_32@163.com

†wu_yong@iapcm.ac.cn

TABLE I. Energies (E; in a.u.) of N^{4+} and N^{3+} states obtained in this work, compared with energies $E_{\rm Ref}$, from NIST [26] and Refs. [10,27]. The values of the energies are given relative to the N^{4+} first ionization threshold (IP = 3.5974 a.u.) which sets the 0 of our scale. Note that the odd (even) parity of a term symbol is indicated by a superscript letter 'o' ('e'); the energies of autoionizing states from Refs. [10], [26], and [27] are distinguished by superscripts 'a', 'b', and 'c', respectively.

N^{4+}							
State	E	$E_{\rm Ref}$ [26]	Δ^*	State	E	$E_{\rm Ref}$ [26]	Δ^*
$1s^22s\ ^2S^e$	−3.5950	−3.5974	0.067%	$1s^24p\ ^2P^o$	−0.7944	−0.7942	0.025%
$1s^22p\ ^2P^o$	−3.2282	−3.2285	0.009%	$1s^24d\ ^2D^e$	−0.7757	−0.7820	0.806%
$1s^23s\ ^2S^e$	−1.5199	−1.5192	0.046%	$1s^24f\ ^2F^o$	−0.7765	−0.7813	0.614%
$1s^23p\ ^2P^o$	−1.4201	−1.4203	0.014%	$1s^25s\ ^2S^e$	−0.5272	−0.5270	0.038%
$1s^23d\ ^2D^e$	−1.3848	−1.3902	0.388%	$1s^25p\ ^2P^o$	−0.5027	−0.5068	0.809%
$1s^24s\ ^2S^e$	−0.8352	−0.8347	0.060%	$1s^25d\ ^2D^e$	−0.4974	−0.5004	0.600%

N^{3+}(bound)				N^{3+}(autoionizing)			
State	E	$E_{\rm Ref}$ [26]	Δ^*	State	E	$E_{\rm Ref}$ [10],^{a} [26],^{b} [27]^c	Δ^*
$1s^22s^2\ ^1S^e$	−6.4382	−6.4445	0.098%	$1s^22p5s\ ^1P^o$	−3.5771	-3.5807^b	0.099%
$1s^22s2p\ ^1P^o$	−5.8355	−5.8490	0.232%	$1s^22p5p\ ^1P^e$	−3.5721	-3.5747^b	0.073%
$1s^22p^2\ ^1D^e$	−5.5731	−5.5839	0.194%	$1s^22p5d\ ^1D^o$	−3.5575	-3.5645^c	0.196%
$1s^22p^2\ ^1S^e$	−5.3559	−5.3721	0.302%	$1s^22p5p\ ^1D^e$	−3.5210	-3.5615^c	1.137%
$1s^22s3s\ ^1S^e$	−4.6699	−4.6728	0.060%	$1s^22p5d\ ^1F^o$	−3.5077	-3.5453^c	1.061%
$1s^22s3p\ ^1P^o$	−4.5983	−4.6014	0.067%	$1s^22p5d\ ^1P^o$	−3.4692	-3.5446^b	2.127%
$1s^22s3d\ ^1D^e$	−4.4789	−4.4891	0.227%	$1s^22p5p\ ^1S^e$	−3.5325	-3.5360^c	0.099%
$1s^22p3s\ ^1P^o$	−4.2859	−4.2892	0.076%	$1s^23s^2\ ^1S^e$	−2.7382	-2.7414^a	0.117%
$1s^22p3p\ ^1P^e$	−4.2513	−4.2535	0.049%	$1s^23s3p\ ^1P^o$	−2.6028	-2.5923^a	0.405%
$1s^22p3d\ ^1D^o$	−4.1676	−4.1740	0.154%	$1s^23s3d\ ^1D^e$	−2.5861	-2.5997^a	0.524%
$1s^22p3p\ ^1D^e$	−4.1632	−4.1677	0.107%	$1s^23p3d\ ^1D^o$	−2.4914	-2.4989^a	0.300%
$1s^22p3d\ ^1F^o$	−4.1272	−4.1377	0.254%	$1s^23p^2\ ^1D^e$	−2.4664	-2.4727^a	0.256%
$1s^22s4p\ ^1P^o$	−4.1303	−4.1343	0.096%	$1s^23p^2\ ^1S^e$	−2.4524	-2.4816^a	1.178%
$1s^22p3p\ ^1S^e$	−4.0898	−4.0954	0.137%	$1s^23p3d\ ^1F^o$	−2.3930	-2.3967^a	0.155%
$1s^22s4d\ ^1D^e$	−4.0828	−4.0951	0.300%	$1s^23d^2\ ^1G^e$	−2.3623	-2.3817^a	0.813%
$1s^22p3d\ ^1P^o$	−4.0729	−4.0816	0.213%	$1s^23p3d\ ^1P^o$	−2.3341	-2.3391^a	0.212%
$1s^22s4f\ ^1F^o$	−4.0438	−4.0667	0.564%	$1s^23d^2\ ^1D^e$	−2.3311	-2.3455^a	0.613%
$1s^22s5s\ ^1S^e$	−3.9501	−3.9534	0.082%	$1s^23d^2\ ^1S^e$	−2.2098	-2.2251^a	0.689%
$1s^22s5p\ ^1P^o$	−3.9340	−3.9375	0.088%	$1s^23s4s\ ^1S^e$	−2.1369	-2.1370^a	0.005%
$1s^22s5d\ ^1D^e$	−3.8564	−3.9189	1.595%	$1s^23s4p\ ^1P^o$	−2.1181	-2.1198^a	0.080%
$1s^22p4s\ ^1P^o$	−3.7932	−3.7981	0.128%	$1s^23s4d\ ^1D^e$	−2.0678	-2.0831^a	0.734%
$1s^22p4p\ ^1P^e$	−3.7786	−3.7806	0.053%	$1s^23s4f\ ^1F^o$	−2.0287	-2.0468^a	0.882%
$1s^22p4d\ ^1D^o$	−3.7485	−3.7623	0.365%	$1s^23p4p\ ^1P^e$	−2.0230	-2.0273^a	0.213%
$1s^22p4d\ ^1F^o$	−3.7191	−3.7515	0.864%	$1s^23p4d\ ^1D^o$	−2.0131	-1.9868^a	1.324%
$1s^22p4p\ ^1D^e$	−3.7380	−3.7515	0.360%	$1s^23p4d\ ^1F^o$	−1.9789	-1.9931^a	0.715%
$1s^22p4p\ ^1S^e$	−3.7292	−3.7372	0.214%	$1s^23p4d\ ^1P^o$	−1.9729	-1.9822^a	0.469%
$1s^22p4d\ ^1P^o$	−3.7040	−3.7174	0.359%	$1s^23p4p\ ^1D^e$	−1.9467	-1.9550^a	0.424%
				$1s^23p4p\ ^1S^e$	−1.9561	-1.9610^a	0.249%
				$1s^23d4d\ ^1F^e$	−1.9540	-1.9497^a	0.221%
				$1s^23d4d\ ^1P^e$	−1.9198	-1.9325^a	0.656%
				$1s^23d4d\ ^1G^e$	−1.9054	-1.8974^a	0.422%
				$1s^23d4d\ ^1D^e$	−1.8865	-1.8915^a	0.265%
				$1s^23d4d\ ^1S^e$	−1.8331	-1.8464^a	0.720%

$^*\Delta = |(E - E_{\rm Ref})/E_{\rm Ref}|$

of DEC and a lack of data for DEC, ADC, and SEC beyond 10 keV/u, except for one series of experimental SEC cross sections [4].

In the present paper, we study theoretically single- and double-electron capture processes in a wide energy domain ranging from 0.25 to 150 keV/u. We use a two-active-electron, three-center, semiclassical, asymptotic-state close-coupling (SCASCC) method with basis sets spanning, among others, the three types of above-mentioned processes. Total and partial SEC cross sections are presented and compared with available theoretical and experimental results. In particular, the contributions of ADC processes to the SEC cross sections and SEC into $N^{4+}(4\ell)$ are analyzed in detail. Furthermore, total DEC cross sections are reported. The discrepancies with previous data are discussed.

The present paper is organized as follows. In the next section we briefly outline the SCASCC method used in the present calculations. Section III is devoted to the detailed

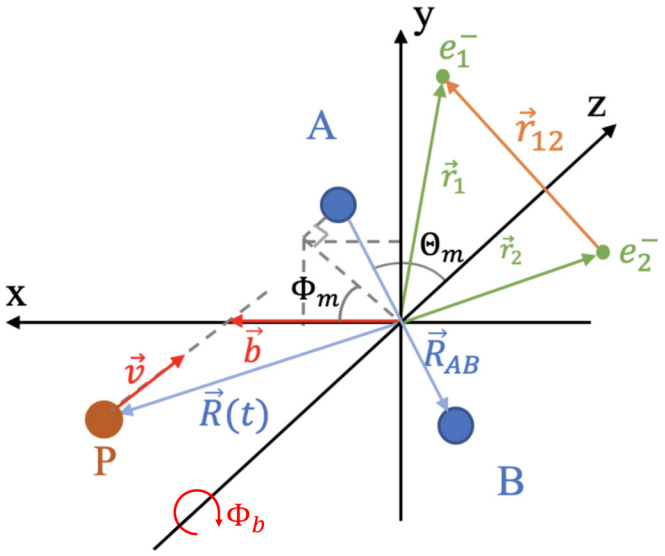

FIG. 1. Collision geometry: the impact parameter $\vec{b}$ and velocity $\vec{v}$ define the collision plane (xOz), where Φ_b is the azimuthal angle used to define the direction of $\vec{b}$ with respect to the x axis (for convenience $\Phi_b = 0$ in the present case). The center of mass of the diatomic molecule defines the origin of the reference frame. The two target nuclei, A and B, are separated by the internuclear vector $\vec{R}_{AB}$. The angles Θ_m and Φ_m define the molecular orientation. The positions of the two electrons are denoted $\vec{r}_1$ and $\vec{r}_2$, and $\vec{r}_{12} = \vec{r}_1 - \vec{r}_2$ is their relative position.

analysis of the total and partial cross sections for SEC, ADC, and DEC processes, including direct comparisons with available experimental and theoretical results. The paper ends with the conclusions of this work in Sec. IV. Atomic units are used throughout, unless explicitly indicated otherwise.

II. THEORY

In the present work, the cross sections of the electronic processes occurring in $N^{5+} + H_2$ collisions are calculated using a two-active-electron, semiclassical, asymptotic-state close-coupling approach which has been previously described in, e.g., [17–20]. Here we only outline the main features of this approach. The two-electron, time-dependent Schrödinger equation is written as

$$\left[H - i\frac{\partial}{\partial t}\bigg|_{\vec{r}_1,\vec{r}_2}\right]\Psi(\vec{r}_1,\vec{r}_2,\vec{R}(t)) = 0, \tag{4}$$

with H the electronic Hamiltonian, defined as

$$H = \sum_{i=1,2}\left[-\frac{1}{2}\nabla_i^2 + V_T(r_i) + V_P\left(r_i^p\right)\right] + \frac{1}{|\vec{r}_1 - \vec{r}_2|}, \tag{5}$$

where $\vec{r}_i$, $\vec{r}_i{}^p = \vec{r}_i - \vec{R}(t)$ are the position vectors of the electrons with respect to the center of mass of the target and to the projectile nuclei, respectively. The relative projectile-target position $\vec{R}(t)$ defines the trajectory in the usual straight-line, constant-velocity approximation, $\vec{R}(t) = \vec{b} + \vec{v}t$, where $\vec{b}$ and $\vec{v}$ are the impact parameter and velocity, respectively (cf. Fig. 1). Note that our approach is based on the rovibrational sudden approximation: the nuclei of the molecular target are frozen (i.e., fixed $\vec{R}_{AB}$). This assumption is valid in the energy range considered in this work since the electronic processes take place on a time scale much shorter (subfemtosecond) than the vibrational motion of the molecular target (>10 fs).

The term V_T (V_P) in Eq. (5) defines the electron-target (electron-projectile) nuclei interaction. For $N^{5+} + H_2$ collisions, these terms are defined as

$$\begin{aligned} V_T(r_i) &= -\frac{1}{\left|\vec{r}_i - \frac{1}{2}\vec{R}_{AB}\right|} - \frac{1}{\left|\vec{r}_i + \frac{1}{2}\vec{R}_{AB}\right|}, \\ V_P\left(r_i^p\right) &= -\frac{5}{r_i^p} - \frac{2}{r_i^p}\left(1 + \alpha\, r_i^p\right)e^{-\beta r_i^p} \end{aligned} \tag{6}$$

in the frozen-core electron approximation employed here, V_P describes the interaction between an active electron and the N^{5+} core (nuclei + inner electrons) ion. The variational parameters $\alpha = 4.3982$ and $\beta = 8.7964$ are taken from [21]. These values were optimized in order to reproduce the N^{4+} spectrum well (see Table I).

The Schrödinger equation, Eq. (4), is solved by expanding the wave function onto a basis set composed by states of the isolated collision partners (i.e., asymptotic states),

$$\begin{aligned} \Psi(\vec{r}_1,\vec{r}_2,\vec{R}(t)) = &\sum_{i=1}^{N_{TT}} c_i^{TT}(t)\Phi_i^{TT}(\vec{r}_1,\vec{r}_2)e^{-iE_i^{TT}t} \\ &+ \sum_{j=1}^{N_{PP}} c_j^{PP}(t)\Phi_j^{PP}(\vec{r}_1,\vec{r}_2)e^{-iE_j^{PP}t} \\ &+ \sum_{k=1}^{N_T}\sum_{l=1}^{N_P} c_{kl}^{TP}(t)\left[\phi_k^T(\vec{r}_1)\phi_l^P(\vec{r}_2,\vec{R}(t))\right. \\ &\left. + \phi_k^T(\vec{r}_2)\phi_l^P(\vec{r}_1,\vec{R}(t))\right]e^{-i(E_k^T + E_l^P)t}, \end{aligned} \tag{7}$$

where the T and TT (P and PP) superscripts denote states (and pseudostates) and corresponding energies for which, respectively, one and two electrons are on the target (projectile). For both electrons, the projectile states contain plane-wave electron translation factors, $e^{i\vec{v}\cdot\vec{r} - i\frac{1}{2}v^2t}$, ensuring Galilean invariance of the results. Note that for the collision system under consideration, the initial state is singlet so that only singlet one- and two-center states are considered in the expansion, Eq. (7). The insertion of Eq. (7) into (4) results in a system of first-order coupled differential equations, which can be written in matrix form as

$$i\frac{\partial}{\partial t}\mathbf{c}(t) = \mathbf{S}^{-1}(\vec{b},\vec{v},t)\mathbf{M}(\vec{b},\vec{v},t)\mathbf{c}(t), \tag{8}$$

where $\mathbf{c}(t)$ is the column vector of the time-dependent expansion coefficients, i.e., c^{TT}, c^{PP}, and c^{TP} in Eq. (7) and $\mathbf{S}$ and $\mathbf{M}$ are the overlap and coupling matrices, respectively. These equations are solved using the predictor-corrector, variable-time-step Adams-Bashford-Moulton method for a set of initial conditions: initial electronic state i, velocity v, impact parameter b, and molecular target orientation defined by (Θ_m, Φ_m) (see Fig. 1).

The probability of a transition $i \to f$ is given by the coefficient c_f ($\equiv c^{TT}$, c^{PP}, or c^{TP}) as

$$P_{fi}(v,\vec{b},R_{AB},\Phi_m,\Theta_m) = \lim_{t\to\infty}|c_f(t)|^2. \tag{9}$$

The corresponding cross sections for a given molecular geometry can be calculated from these probabilities as

$$\sigma_{fi}(v, R_{AB}, \Theta_m) = \int d^2\vec{b} P_{fi}(v, \vec{b}, R_{AB}, \Phi_m, \Theta_m), \quad (10)$$

where the dependence upon Φ_m disappears after integration over $\vec{b}$. The total cross sections (averaged over the degrees of freedom of the molecule) are then given by

$$\sigma_{fi}^{\rm tot}(v) = \int_0^{\pi}\int_0^{\infty} \rho(\Theta_m)\rho(R_{AB}) \times \sigma_{fi}(v, R_{AB}, \Theta_m) dR_{AB} d\Theta_m, \quad (11)$$

where $\rho(\Theta_m)$ and $\rho(R_{AB})$ are, respectively, the distribution of the molecular geometry over Θ_m and R_{AB}. The former is assumed to be isotropic, i.e.,

$$\rho(\Theta_m) = \tfrac{1}{2}\sin(\Theta_m). \quad (12)$$

The distribution $\rho(R_{AB})$ over the internuclear distance of the target is generally that corresponding to a given (e.g., ground) vibrational state or a superposition of vibrational states of the molecular target [22]. The cross sections should then be evaluated for different values of R_{AB} and generally averaged over the initial vibrational state distribution. However, it has been shown that considering only the equilibrium distance value $R_{\rm eq}$ is sufficient to obtain accurate cross sections [17,22–24]. In the following we therefore consider only a molecular target frozen at the equilibrium distance, the so-called Franck-Condon approximation (cf. [25]). $\rho(R_{AB})$ is thus expressed as

$$\rho(R_{AB}) = \delta(R_{AB} - R_{\rm eq}), \quad (13)$$

where $R_{\rm eq} = 1.4$ a.u. for H_2.

The total cross sections [Eq. (11)] can be rewritten as

$$\sigma_{fi}^{\rm tot}(v) = \frac{1}{2}\int_0^{\pi} d\Theta_m \sin(\Theta_m)\sigma_{fi}(v, R_{\rm eq}, \Theta_m). \quad (14)$$

In order to reduce the computational costs, it is often chosen to evaluate the cross sections through an approximate averaging procedure using only three characteristic molecular orientations, namely, $(\Theta_m, \Phi_m) = (0, 0),\ (\pi/2, 0),\ (\pi/2, \pi/2)$,

$$\sigma_{fi}^{\rm tot}(v, R_{\rm eq}) = \frac{2\pi}{3}[\varrho_{fi}(v, R_{\rm eq}, 0, 0) + \varrho_{fi}(v, R_{\rm eq}, \pi/2, 0) + \varrho_{fi}(v, R_{\rm eq}, \pi/2, \pi/2)], \quad (15)$$

with

$$\varrho_{fi}(v, R_{\rm eq}, \Theta_m, \Phi_m) = \int_0^{+\infty} bP_{fi}(v, b, R_{\rm eq}, \Theta_m, \Phi_m) db. \quad (16)$$

This approximation has been widely used and proven to give good estimates of the cross sections [17,23–25].

In our calculations, the one- and two-electron states and pseudostates included in the expansion, Eq. (7), are expressed in terms of Gaussian-type orbitals (GTOs) and of products of these GTOs. For the system under consideration, a set of 70 GTOs (12 for $\ell = 0$, 8×3 for $\ell = 1$, 4×5 for $\ell = 2$, and 2×7 for $\ell = 3$) is used on the N^{5+} center and 7 GTOs for $\ell = 0$ taken from [17] are used for each center of H_2. In the wave-function expansion, we have included 3074 singlet states and pseudostates in total: 53 TT (H_2), 681 TP (H_2^+, N^{4+}), and 2340 PP (N^{3+}) ones. In Table I, we list the energies of the relevant N^{4+} and N^{3+} states compared with the corresponding available data from NIST [26] and Refs. [10,27]. The overall agreement between our calculated energies and the available data is excellent for the main states under consideration in the following and, at worst, equal to about 2% for the doubly excited autoionizing states.

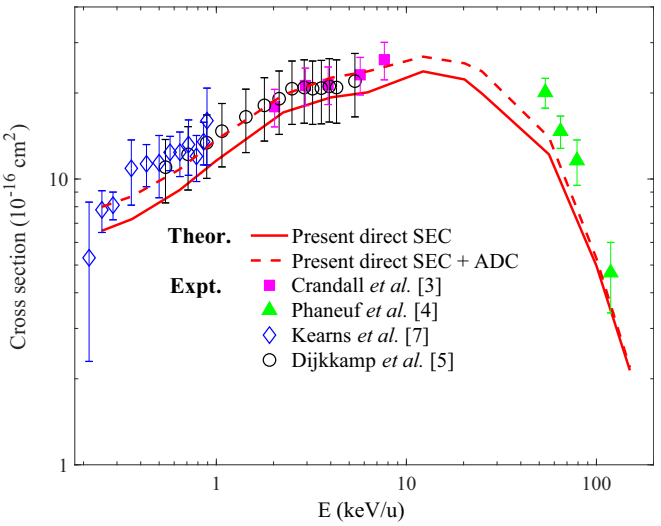

FIG. 2. Single-electron capture cross sections as a function of the impact energy. The present calculations for direct SEC to N^{4+} are denoted by the solid red line; the total SEC cross sections (direct SEC + ADC) are denoted by the dashed red line. The experimental results are from Crandall *et al.* [3] (filled magenta squares), Phaneuf *et al.* [4] (filled green triangles), Dijkkamp *et al.* [5] (open black circles), and Kearns *et al.* [7] (open blue diamonds).

The results reported in the following have been compared with those from a smaller basis set built from 53 GTOs (10 for $\ell = 0$, 7×3 for $\ell = 1$, 3×5 for $\ell = 2$, and 1×7 for $\ell = 3$) on the N^{5+} center and 5 GTOs for $\ell = 0$ on each center of the H_2 target. The SEC cross sections from these two sets agree with each other within 10%, except for the weakest channels [e.g., SEC to $N^{4+}(1s^2 3s)$ and $N^{4+}(1s^2 4s)$] at the highest impact energy (150 keV/u), for which differences reach about 30%. For the two-electron processes (DEC and ADC), the cross sections differ by less than 10% at intermediate energies and by less than 30% at low and high impact energies. Note that the difference between the cross sections for ADC to $N^{3+}(2p5\ell)$ obtained with the two basis sets reaches a maximum of 70% at high impact energies. However, the values of the cross sections are rather small (around 10^{-18} cm^2).

III. RESULTS AND DISCUSSION

A. Total single-electron capture (single-projectile charge-changing) cross sections

In Fig. 2, our single-electron capture cross sections for $N^{5+} + H_2$ collisions are presented in the energy region from 0.25 to 150 keV/u, together with available experimental data [3–5,7]. We first discuss the results of direct SEC, i.e., including only the three processes listed in Eqs. (1). The

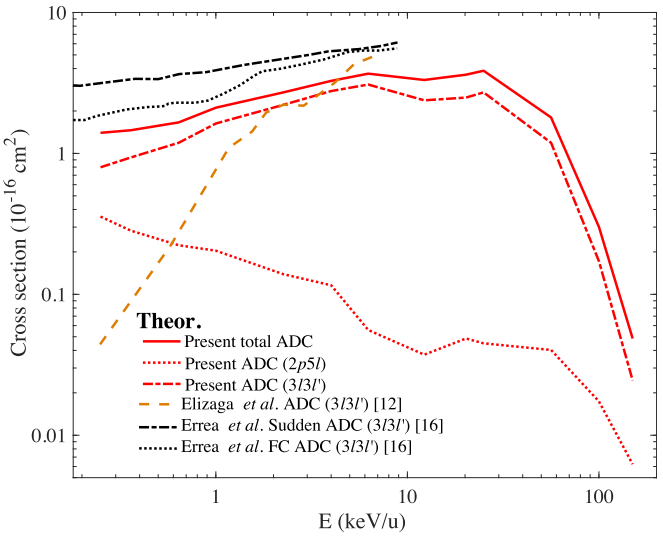

FIG. 3. Total and shell-resolved ADC cross sections as a function of the impact energy. The present calculations for total ADC are denoted by the solid red line. The present results for shell-resolved ADC to $N^{3+}(2p5\ell)$ are represented by the dotted red line and to $N^{3+}(3\ell3\ell')$ by the dash-dotted red line. Theoretical calculations of $N^{3+}(3\ell3\ell')$ from Elizaga *et al.* [12] (dashed orange line) and Errea *et al.* [16] (dash-dotted black line) for the sudden approximation and (dotted black line) for the Franck-Condon (FC) approximation, respectively.

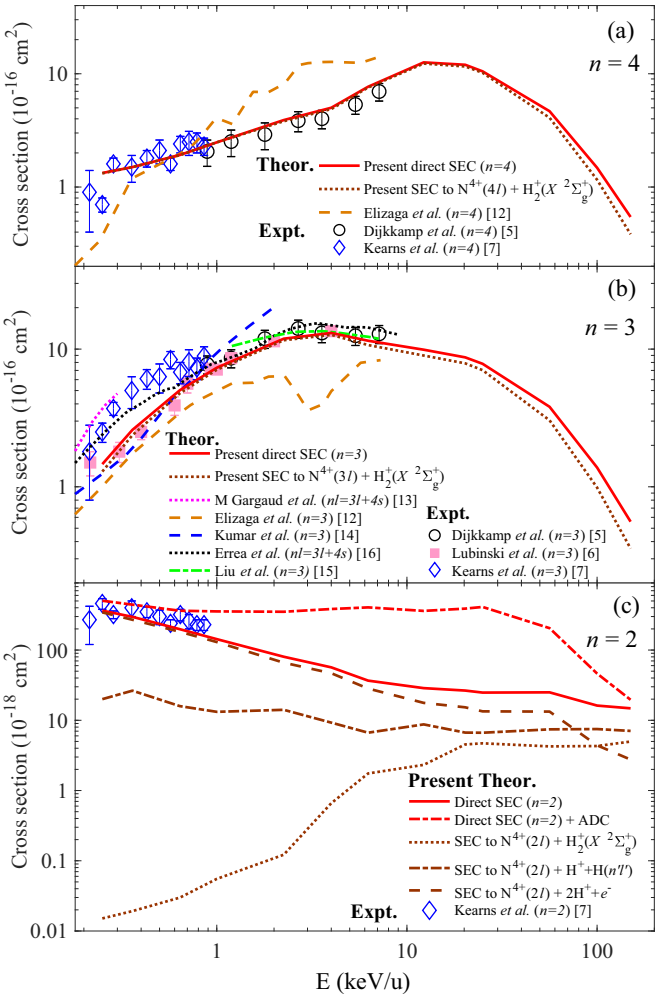

FIG. 4. Shell-resolved SEC cross sections as a function of the impact energy: for $n = 4$ (a), $n = 3$ (b), and $n = 2$ (c). The direct SEC cross sections are shown as solid red lines, while the total (direct + ADC) SEC cross sections are shown as the dash-dotted red line in (c). The calculations of Kumar *et al.* [14] are denoted by the dashed blue line; the results of Elizaga *et al.* [12], by the dashed orange line; and those of Liu *et al.* [15], by the dash-dotted green line. The results for SEC to N^{4+} ($n\ell = 3\ell + 4s$) of Gargaud *et al.* [13] are indicated by the dotted magenta line and those of Errea *et al.* [16] by the dotted black line. The experimental results of Dijkkamp *et al.* [5] are represented by open black circles; those of Lubinski *et al.* [6], by filled pink squares; and those of Kearns *et al.* [7], by open blue diamonds.

cross sections increase steadily to a maximum located at about 12 keV/u and drop rapidly for increasing energies. A shoulder can be seen at about 3 keV/u and comes from the interplay of the single-electron capture into $n = 3$ and $n = 4$, whose cross sections exhibit a maximum at different collision energies, as shown in Fig. 4.

Compared with the available experimental data, our results lie somewhat lower than the experimental results of Crandall *et al.* [3], Dijkkamp *et al.* [5], and Kearns *et al.* [7] at low energies and of Phaneuf *et al.* [4], the unique available experimental investigation at energies $E > 10$ keV/u. However, the doubly excited $N^{3+}(1s^2n\ell n'\ell')$ states populated by double-electron transfer decay to $N^{4+}(1s^22\ell)$ before being detected experimentally, due to their extremely short lifetimes [10,11]. The measured total SEC (projectile charge-changing) cross sections therefore correspond to the sum of the direct SEC cross sections and the ADC ones. Our total SEC cross sections are represented by the dashed red line in Fig. 2 and show an excellent agreement with the experimental data [3,5,7] in the low-energy range. Our calculations indicate that the ADC contribution in the measured SEC cross sections is about 20% at the lowest impact energy we considered, while it becomes less important as the impact energy increases. However, at high energies, a disagreement remains with the experimental cross sections of Phaneuf *et al.* [4].

B. Double-capture to autoionizing states

In order to gain more insights into the total SEC processes, we report in Fig. 3 the total and partial ADC cross sections as a function of the impact energy. Our calculations are compared with the previous theoretical investigations by Elizaga *et al.* [12] and Errea *et al.* [16]. Our results show that ADC to $N^{3+}(1s^23\ell3\ell')$ are dominant in the whole energy region. It can be seen in Fig. 3 that the related cross sections from Errea *et al.* [16] using both Franck-Condon and sudden approximations are larger than the present total ADC ones but show a similar dependence as a function of the energy. However, a very poor agreement between the present cross sections and the independent particle model results [12] is seen. These discrepancies might be due to the independent particle model and isotropic molecular target approximations used in [12] as well as the limited size of the basis set in [16], as mentioned in Sec. IV. Indeed, in the latter work,

the authors included only 17 channels in total. In the present work, we use a much larger wave-function expansion spanning more SEC, ADC, and DEC channels: among others, SEC and TE channels correlated with $N^{4+}(1s^24p)$, $N^{4+}(1s^24d)$, and $N^{4+}(1s^24f)$ states and ADC channels corresponding to states above $N^{3+}(1s^23p^2)$, which were not considered in [16]. Furthermore, we recall that the uncertainty of our cross sections due to the size of our basis set is expected to be less than 30%, i.e., smaller than the observed discrepancies. We therefore believe that our calculations provide, to date, the most accurate ADC cross sections.

We show also in Fig. 3 the cross sections of ADC to $N^{3+}(1s^22p5\ell)$. These are negligible at high energies, contributing only about 5% to ADC at 50 keV/u where the cross sections show a shallow peak, reaching values only about a factor of 4 smaller than the total ADC cross sections at 0.25 keV/u. This behavior is actually in accordance with the electron spectrum measured for collisions of N^{5+} with H_2 [28,29], where the relative intensity of the decay from $N^{3+}(1s^22p n\ell)$ states by Coster-Kronig transitions increases with decreasing impact energies.

Finally, the present ADC cross sections can be compared to those of the isocharged, fully stripped projectile B^{5+}-H_2 collision system [30]. Even though more autoionizing states are available (e.g., the $2sn\ell\ ^{2S+1}L$ states) for B^{3+}, compared to N^{3+}, the present cross sections are a factor of 5 larger [30]. This significant difference is related to the general shift towards a higher binding energy of the low-angular-momentum states for N^{q+} ($q < 5$), due to the only partial screening of the K electrons.

C. *n*-selective single-electron capture

We now investigate shell-resolved cross sections for the direct single-electron capture processes in Eqs. (1). Such detailed information on the final-state distribution of captured electrons is of particular interest both in astrophysics and in plasma diagnostics research, since it determines the characteristics of the emitted radiation.

Our shell-resolved cross sections for SEC to N^{4+} ($n = 2, 3, 4$) are presented in Fig. 4, together with the available experimental [5–7] and theoretical [12–16] data. Our results show that the cross sections for SEC to N^{4+} ($n = 2$) are dominant for energies lower than 0.5 keV/u, while the cross sections for SEC to N^{4+} ($n = 3$) take over up to 10 keV/u. At higher impact energies, for which no other data exist, the cross sections for SEC to N^{4+} ($n = 3$ and 4) become comparable.

For the cross sections of SEC to N^{4+}($n = 4$) in Fig. 4(a), our results are in good agreement with the experimental data of Dijkkamp *et al.* [5] and Kearns *et al.* [7] in the respective overlapping energies. The independent particle model results of Elizaga *et al.* [12] lie above the experimental data [5] for $E > 10$ keV/u but below the experimental cross sections [7] for $E < 3$ keV/u. These disagreements suggest that electronic correlations play an important role in the present collision system.

For the cross sections of SEC to N^{4+} ($n = 3$), it can be observed in Fig. 4(b) that our results agree well with the experimental results [5,6], as well as with the SCMOCC calculations by Errea *et al.* [16] and with the single-electron, atomic-orbital close-coupling (SCAOCC) calculations by Liu *et al.* [15] for $E > 0.8$ keV/u. However in this range, the theoretical predictions of Elizaga *et al.* [12] and Kumar *et al.* [14] underestimate and overestimate, respectively, the five sets of converging data. In the latter, SCMOCC investigations [14], SEC to N^{4+} ($n = 4$) channels were not taken into account in the calculations, which may explain the overestimation of the cross sections of SEC to N^{4+} ($n = 3$) since these two channels are similarly likely in this close-coupling regime.

For $E < 0.8$ keV/u, our N^{4+} ($n = 3$) results are in good agreement with the experimental results of Lubinski *et al.* [6]. However, the experimental results of Kearns *et al.* [7] lie slightly above, in somehow reasonable agreement with the molecular calculations by Errea *et al.* [16] and Gargaud *et al.* [13]. As discussed in [7], the authors could not give a clear quantitative assessment of cross sections for SEC to N^{4+} ($n = 3$) and N^{4+} ($n = 2$) in their measurements due to the overlap in the energy defects of the two processes; see Eq. (3) for $n = 3$ and Eq. (6a) for $n = 2$ (via ADC) in [7]. Their cross sections of SEC to N^{4+} ($n = 3$) might then be overestimated, while the cross sections of SEC to N^{4+} ($n = 2$) are underestimated. This could explain the disagreement with our results. This explanation is further supported by the comparison of the cross sections of SEC to N^{4+} ($n = 2$) (see below).

In Fig. 4(c), our cross sections for SEC to N^{4+} ($n = 2$) are compared with the only available experimental [7] results. Our results for direct SEC to N^{4+} ($n = 2$) (solid red line) are slightly smaller than the experimental ones. However, as mentioned before, in [7], the ADC contributions could not be separated from the direct SEC processes. Therefore we also include in Fig. 4(c) the cross sections for the total SEC to N^{4+} ($n = 2$) (dash-dotted red line). These cross sections are slightly larger than the experimental data from [7]. As discussed for the cross sections of SEC to N^{4+} ($n = 3$), this disagreement may come from the overlap in the energy defects of the SEC to N^{4+} ($n = 2$ and 3) reported in [7].

Before discussing $n\ell$-selective single-electron capture, we mention that the cross sections of SEC to N^{4+} ($n = 3$ and 4) are mostly (>95%) related to a true one-electron process for which the ionized target ends up in the ground state, i.e., nondissociative SEC, Eq. (1b) [see dotted brown lines in Figs. 4(a) and 4(b)]. However, as shown in Fig. 4(c), the SEC to N^{4+} ($n = 2$) shows a different behavior: in the low-energy range, more than 80% of the contribution of the cross sections appears to stem from two-electron transfer excitation and ionization dissociative processes of Eqs. 1(b) and 1(c) (dash-dotted and dashed brown lines), where, in particular, the cross section for nondissociative SEC is negligible small. In contrast, at high energies direct (nondissociative) SEC, Eq. 1(a), becomes comparable with transfer excitation ones, Eq. 1(c), both of them showing oscillatory structures with opposite phases, which tend to indicate that they are strongly coupled. These results related to the contribution of dissociative and nondissociative processes are in agreement with the experimental investigations in [6,7].

We also note here that the discrepancies observed at low collision energies and the lack of data at higher energies demonstrate that further experimental works are needed.

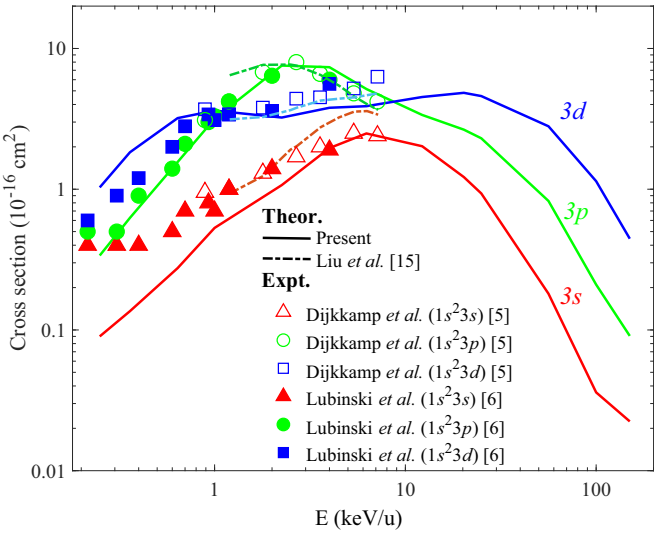

FIG. 5. The 3ℓ-resolved SEC cross sections as a function of the impact energy. The present results are shown by solid lines; these of Liu *et al.* [15], by the dash-dotted line. The experimental data are from Dijkkamp *et al.* [5] (open symbols) and Lubinski *et al.* [6] (filled symbols).

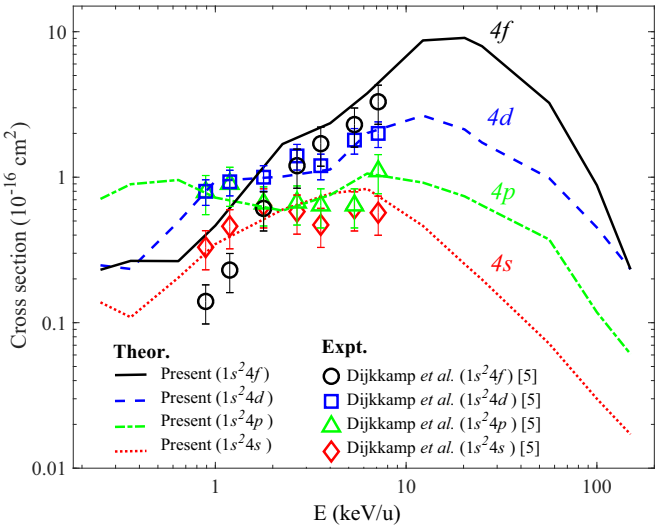

FIG. 6. The 4ℓ-selective SEC cross sections as a function of the impact energy. The present results are denoted by lines; the experimental results of Dijkkamp *et al.* [5], by symbols.

D. $n\ell$-selective single-electron capture

We now investigate subshell-resolved electron capture cross sections. Our 3ℓ-resolved SEC cross sections are presented in Fig. 5, together with the experimental results from [5,6] and the single-electron SCAOCC calculations by Liu *et al.* [15] for comparison. As displayed in Fig. 5, the cross sections of the clearly dominant $N^{4+}(1s^2 3p)$ and $N^{4+}(1s^2 3d)$ channels follow a complex behavior as a function of the energy. Indeed electron capture to the $N^{4+}(1s^2 3p)$ state dominates only in the narrow energy region 1–9 keV/u. For this channel, our results are in excellent agreement with the experimental data [5,6] and the calculations [15] in the whole overlapping energies. For the SEC-to-$N^{4+}(1s^2 3d)$ channel, our results are also in good agreement with the available data [5,6,15], only slightly underestimating (overestimating) the experimental data for $E > 5$ keV/u ($E < 0.6$ keV/u). For the weakest channel, electron capture to $N^{4+}(1s^2 3s)$ states, our calculations agree with the experimental data [5,6] at the maximum of the cross sections but are systematically lower for decreasing energies.

In Fig. 6, our 4ℓ-resolved SEC cross sections are presented and compared with the experimental data of Dijkkamp *et al.* [5]. Our results show that the cross sections for SEC to $N^{4+}(1s^2 4f)$ play a predominant role for energies higher than 2 keV/u, with a maximum at 20 keV/u. For decreasing energies, SEC to $N^{4+}(1s^2 4d)$ and $N^{4+}(1s^2 4p)$ becomes dominant. As shown in Fig. 6, our results for electron capture to $N^{4+}(1s^2 4s$, $1s^2 4p$, and $1s^2 4d)$ are in very good agreement with these of Dijkkamp *et al.* [5]. For the $N^{4+}(1s^2 4f)$ channel, our calculations also agree well with the experimental data [5] for $E > 2$ keV. At lower collision energies, our cross sections are larger than the experimental ones. Further investigations are still required to make conclusions on this discrepancy.

E. Double-electron capture

In Fig. 7, our cross sections of total and partial double-electron capture to bound states, Eq. (2), are presented, together with the only four available experimental data points from [3] and the theoretical calculations from [12]. The experimental results show that the DEC cross sections are of the same order of magnitude as the present ADC ones and one order of magnitude smaller than the SEC ones. However, our results are nearly one order of magnitude below the experimental data [3], showing a weak increase up to a broad

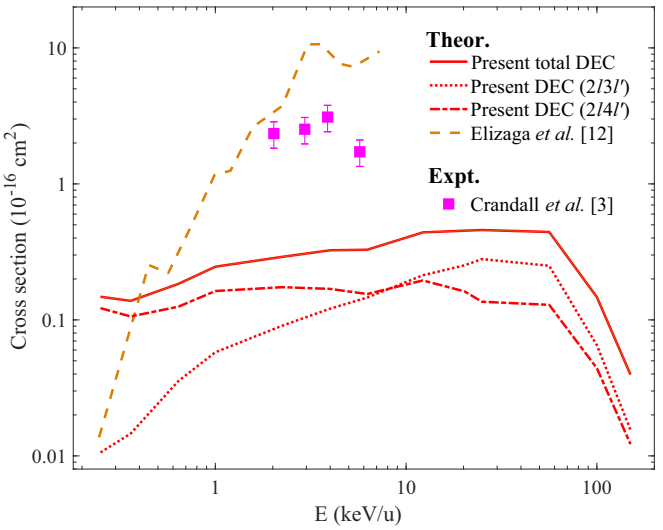

FIG. 7. Total and shell-resolved DEC cross sections as a function of the impact energy. The present calculations for total DEC are denoted by the solid line. Present results for shell-resolved DEC to N^{3+} ($2\ell 3\ell'$) and N^{3+} ($2\ell 4\ell'$) are represented by the dotted line and dash-dotted line, respectively. The theoretical results of Elizaga *et al.* [12] are shown by the dashed line; the experimental data of Crandall *et al.* [3], by filled squares.

maximum around 50 keV/u, followed by a rapid decay. As displayed in Fig. 7, none of the results agree with each other, the other theoretical prediction [12] being above the experimental data. Obviously, a large discrepancy exists between the experimental data [3] and our calculations. Note, however, that in [3], the presence of long-lived excited states of N^{5+} in the incoming beam could not be ruled out. Such excited states may have large cross sections and thus produce a significant enhancement in the measured DEC cross sections. Further theoretical and experimental investigations will be useful to draw definite conclusions.

For completeness, we show the shell-resolved cross sections of the dominant DEC channels, i.e., $N^{3+}(1s^2 2\ell 3\ell')$ and $N^{3+}(1s^2 2\ell 4\ell')$, in Fig. 7. Our results show that the cross section for DEC to $N^{3+}(1s^2 2\ell 4\ell')$ dominates up to 10 keV/u, while DEC to $N^{3+}(1s^2 2\ell 3\ell')$ takes over from there. The sum of these two cross sections leads to a shoulder in the total DEC cross sections at around 3 keV/u as in the SEC case.

IV. CONCLUSION

In this paper, one- and two-electron processes occurring in the course of $N^{5+} + H_2$ collisions have been investigated using a two-active-electron, three-center, semiclassical, asymptotic-state nonperturbative method over a wide collision energy range. To date, our close-coupling description of the collision is the most elaborated one, in terms of accounting for electron correlation, molecular structures, and active channels. For single-electron capture processes, our results are, in general, in good agreement with the experimental ones. The few discrepancies are discussed. Furthermore, our work provides single-electron capture cross sections, beyond 10 keV/u impact energies and up to 150 keV/u, where no other data were previously available. In contrast to single-electron capture, there are large discrepancies between our results and the rare existing experimental and theoretical results for the double-electron capture cross sections.

Despite the extensive literature on electron capture processes in $N^{5+} + H_2$ collisions, this system remains challenging. Further theoretical and experimental investigations on single- and double-electron capture processes are needed. Our work provides insights into these electronic processes and new data which are essential to improve our understanding of this relevant collisional system.

ACKNOWLEDGMENTS

This work was supported by the National Natural Science Foundation of China (Grants No. 11934004 and No.11704040) and the National Key Research and Development Program of China (Grant No. 2017YFA0402300). This project received funding from the LABEX Plas@par (Grant No. ANR-11-IDEX-0004-02).

[1] T. E. Cravens, Sci. **296**, 1042 (2002).
[2] R. Janev, *Atomic and Plasma-Material Interaction Data for Fusion* (International Atomic Energy Agency, Vienna, Austria, 2001).
[3] D. H. Crandall, M. L. Mallory, and D. C. Kocher, Phys. Rev. A **15**, 61 (1977).
[4] R. A. Phaneuf, F. W. Meyer, and R. H. McKnight, Phys. Rev. A **17**, 534 (1978).
[5] D. Dijkkamp, D. Ciric, E. Vileg, A. de Boer, and F. J. de Heer, J. Phys. B **18**, 4763 (1985).
[6] G. Lubinski, Z. Juhász, R. Morgenstern, and R. Hoekstra, J. Phys. B **33**, 5275 (2000).
[7] D. M. Kearns, R. W. McCullough, and H. B. Gilbody, J. Phys. B **35**, 4335 (2002).
[8] Note that some of these investigations reported charge-changing cross sections and therefore address processes other than single-electron transfer.
[9] A. Bordenave-Montesquieu, M. Boudjema, P. Benoit-Cattin, A. Gleizes, and P. Moretto-Capelle, J. Phys. Colloq. **50**, 305 (1989).
[10] H. Bachau, P. Galan, F. Martin, A. Riera, and M. Yanez, At. Data Nucl. Data **44**, 305 (1990).
[11] N. Nakamura, H. Ida, Y. Matsui, K. Wakiya, T. Takayanagi, M. Koide, F. Currell, S. Kitazawa, H. Suzuki, S. Ohtani, U. Safronova, and M. Sekiguchi, J. Phys. B **31**, 3233 (1998).
[12] D. Elizaga, L. Errea, A. Macías, L. Méndez, A. Riera, and A. Rojas, Phys. Scripta **1999**, 187 (1999).
[13] M. Gargaud and R. McCarroll, J. Phys. B **18**, 463 (1985).
[14] A. Kumar and B. C. Saha, Phys. Rev. A **59**, 1273 (1999).
[15] L. Liu, Y. Q. Zhao, J. G. Wang, R. K. Janev, and H. Tanuma, Phys. Rev. A **81**, 014702 (2010).
[16] L. F. Errea, L. Fernández, A. Macías, L. Méndez, I. Rabadán, and A. Riera, Phys. Rev. A **69**, 012705 (2004).
[17] N. Sisourat, I. Pilskog, and A. Dubois, Phys. Rev. A **84**, 052722 (2011).
[18] J. W. Gao, Y. Wu, N. Sisourat, J. G. Wang, and A. Dubois, Phys. Rev. A **96**, 052703 (2017).
[19] J. W. Gao, Y. Wu, J. G. Wang, N. Sisourat, and A. Dubois, Phys. Rev. A **97**, 052709 (2018).
[20] J. W. Gao, Y. Wu, J. G. Wang, A. Dubois, and N. Sisourat, Phys. Rev. Lett. **122**, 093402 (2019).
[21] L. Errea, A. Macías, L. Méndez, I. Rabadán, A. Riera, and P. Sanz, Int. J. Quantum Chem. **86**, 182 (2002).
[22] J. Caillat, A. Dubois, I. Sundvor, and J. P. Hansen, Phys. Rev. A **70**, 032715 (2004).
[23] J. Caillat, N. Sisourat, A. Dubois, I. Sundvor, and J. P. Hansen, Phys. Rev. A **73**, 014701 (2006).
[24] I. Rabadán, L. Méndez, J. W. Gao, Y. Wu, and J. G. Wang, Phys. Rev. A **96**, 032714 (2017).
[25] L. Errea, J. Gorfinkiel, A. Macías, L. Méndez, and A. Riera, J. Phys. B **30**, 3855 (1997).
[26] A. Kramida, Yu. Ralchenko, J. Reader, and NIST ASD Team, *NIST Atomic Spectra Database (Version 5.6.1)* (National Institute of Standards and Technology, Gaithersburg, MD, 2018), Available at: https://physics.nist.gov/asd.
[27] K. Aggarwal, F. Keenan, and K. Lawson, Mon. Not. R. Astron. Soc. **461**, 3997 (2016).
[28] E. M. Mack, Nucl. Instrum. Methods **B32**, 74 (1987).
[29] E. M. Mack, Electron capture to autoionizing states of multiply charged ions, Ph.D. thesis, University of Utrech, 1987.
[30] I. Pilskog, N. Sisourat, J. Caillat, and A. Dubois, Phys. Rev. A **85**, 042712 (2012).